Dependence of the efficiency of spin Hall torque on the transparency of Pt/ferromagnetic layer interfaces

Chi-Feng Pai, Yongxi Ou, Luis Henrique Vilela-Leão, D. C. Ralph, and R. A. Buhrman

Phys. Rev. B **92**, 064426 — Published 31 August 2015

DOI: 10.1103/PhysRevB.92.064426

Dependence of the Efficiency of Spin Hall Torque on the Transparency of Pt/Ferromagnetic Layer Interfaces

Chi-Feng Pai[1†], Yongxi Ou[1], Luis Henrique Vilela-Leão[1‡], D. C. Ralph[1,2], and R. A. Buhrman[1,*]

[1]Cornell University, Ithaca, New York 14853, USA

[2]Kavli Institute at Cornell, Ithaca, New York 14853, USA

[†]Current Affiliation: Massachusetts Institute of Technology, Cambridge, Massachusetts 02139, USA

[‡]Current Affiliation: Centro Acadêmico do Agreste, Universidade Federal de Pernambuco, 55002-970 Caruaru, PE, Brazil

We report that spin current transport across Pt/ferromagnet (FM) interfaces as measured by the spin torques exerted on the FM is strongly dependent on the type and the thickness of the FM layer and on post-deposition processing protocols. By employing both harmonic voltage measurements and spin-torque ferromagnetic resonance measurements, we find that the efficiency of the Pt spin Hall effect in exerting a damping-like spin torque on the FM corresponds to an effective spin Hall ratio ranging from < 0.05 to > 0.10 under different interfacial conditions. The "internal" spin Hall ratio of the Pt thin films used in this study, after taking the interfacial spin transmission factor into account, is estimated to be ~ 0.30. This suggests that a careful engineering of Pt/FM interfaces can improve the spin-Hall-torque efficiency of Pt-based spintronic devices. We also note that the dependence on temperature for both vector components of the spin-Hall torque is strongly dependent on the details of the Pt/FM interface, and that measurements of magnetic damping as a function of FM layer thickness are not generally reliable for determining the true effective spin mixing conductance for the interface.

The spin Hall effect (SHE) [1, 2] causes an electrical current density J_e flowing through a material with strong spin-orbit interactions to generate a transverse spin current density J_s. The amplitude of J_s is characterized by the spin Hall ratio (or spin Hall angle) $\theta_{\mathrm{SH}} \equiv (2e/\hbar)J_s/J_e$. The most straightforward way to determine a lower bound [3], $\theta_{\mathrm{SH}}^{\mathrm{LB}}$, on the spin Hall ratio in normal metal (NM) systems is to measure the current-dependent torque that is exerted on an adjacent ferromagnet (FM) when spin current flows to the NM/FM interface. This spin torque is also currently the most technologically promising aspect of the SHE. Research has shown [4, 5] that there are two different components of torque that can be observed in this case: a "damping-like" torque $\vec{\tau}_{DL} \propto J_e \hat{m} \times (\hat{\sigma} \times \hat{m})$, where $\hat{m}$ is the orientation of the ferromagnetic moment, and a "field-like" torque $\vec{\tau}_{FL} \propto -J_e \hat{\sigma} \times \hat{m}$. The determination via τ_{DL} measurements of a large $\theta_{\mathrm{SH}}^{\mathrm{LB}} \approx 0.07$, in Pt/FM thin film bilayers [3, 6, 7], and the subsequent observation of even larger, "giant" spin Hall ratio for high resistivity Ta (amorphous or β-phase Ta), $\left|\theta_{\mathrm{SH}}^{\mathrm{LB}}\right| \approx 0.12$ [8] and β-W, $\left|\theta_{\mathrm{SH}}^{\mathrm{LB}}\right| \approx 0.33$ [9, 10], have opened up a very active area for research and technology development. There is of course the possibility of an additional source of spin-orbit torques that could arise from a spin-orbit interaction of the applied current at the NM/FM interface [11-14]. However, it has also been demonstrated that both spin-orbit torques decrease when a spacer layer is inserted between the heavy metal and the FM [10, 15]. This strongly suggests that the spin current generated by the SHE in the NM is the principal origin of these effects in most cases including Pt [16], although certainly the interface plays an essential role in determining the strength and character of the resultant torques, as we discuss here.

As indicated above, measurement of the spin torque that is exerted on any particular FM layer by a J_e flowing in the adjacent NM provides only a lower bound on the strength of the J_s that is generated internally in the NM [7]. This is because the spin transmission probability of the NM|FM

interface will generally be less than unity. This reduction in interfacial spin transparency may arise from at least two effects. First, theoretical studies indicate there will be spin backflow (SBF) even from a well-ordered, abrupt interface whose strength depends on the "spin-mixing conductance" $G^{\uparrow\downarrow}$ of the interface relative to the spin conductance of the NM G_{NM} [13]. Second, if the interface is formed in such a manner that there is an interfacial layer in which there is an enhanced rate of spin scattering, this can result in spin memory loss (SML) [17, 18], which may also reduce the transmitted spin current. This enhanced spin scattering could be due to intermixing and disorder at the NM/FM interface or perhaps to a magnetic proximity effect in the first few layers of the Pt [19]. Whether SBF or SML is the dominant factor, or whether both factors are important, this reduction in the transmitted spin current can be characterized, as suggested above, by defining a damping-like spin torque efficiency ξ_{DL}, and also a field-like torque efficiency ξ_{FL}, for a particular NM/FM interface, such that ξ_{DL} must be less than or equal to the "internal" spin Hall angle θ_{SH} that quantifies the spin current generated within the NM. The accumulating reports [20-25] that ξ_{DL} can be quite variable for Pt/FM systems, and in some cases is > 0.07, strongly suggest that the composition and preparation of the Pt/FM bilayer is playing a major role in determining the spin torque efficiency and also, as discussed below and in recent works [26, 27], that the internal spin Hall ratio of Pt is likely significantly greater than the lower bound initially reported, $\theta_{\mathrm{SH}}^{\mathrm{LB}} = 0.07$ [3]. If this is correct it points to the opportunity to develop interface-engineering protocols that might better maximize ξ_{DL} for applications.

In the absence of significant SML, recent calculations utilizing the drift-diffusion approximation [13, 28], have determined that the effects of spin backflow should reduce the spin torque efficiencies as

$$\xi_{DL} = \theta_{\mathrm{SH}} \,\mathrm{Re}\left\{\frac{2G^{\uparrow\downarrow}\tanh\left(\frac{d_{\mathrm{NM}}}{2\lambda_{\mathrm{s,NM}}}\right)}{G_{\mathrm{NM}} + 2G^{\uparrow\downarrow}\coth\left(\frac{d_{\mathrm{NM}}}{\lambda_{\mathrm{s,NM}}}\right)}\right\}, \text{ and } \xi_{FL} = \theta_{\mathrm{SH}} \,\mathrm{Im}\left\{\frac{2G^{\uparrow\downarrow}\tanh\left(\frac{d_{\mathrm{NM}}}{2\lambda_{\mathrm{s,NM}}}\right)}{G_{\mathrm{NM}} + 2G^{\uparrow\downarrow}\coth\left(\frac{d_{\mathrm{NM}}}{\lambda_{\mathrm{s,NM}}}\right)}\right\}. \quad (1)$$

Here the spin conductance of the NM $G_{\mathrm{NM}} \equiv \sigma_{\mathrm{NM}} / \lambda_{\mathrm{s,NM}}$, where σ_{NM} and $\lambda_{\mathrm{s,NM}}$ represent the conductivity and the spin diffusion length, respectively, and d_{NM} is the NM layer thickness. $G^{\uparrow\downarrow}$ is the bare spin-mixing conductance of the interface [29, 30]. If we assume $d_{\mathrm{NM}} >> \lambda_{\mathrm{s,NM}}$ and that $\mathrm{Re}\,G^{\uparrow\downarrow} >> \mathrm{Im}\,G^{\uparrow\downarrow}$ as is expected to be the case for NM/FM interfaces with a sufficiently thick FM [30], then from Eqn. (1) we have

$$\xi_{DL} = \theta_{\mathrm{SH}}\left(2G^{\uparrow\downarrow} / G_{\mathrm{NM}}\right) / \left(1 + 2G^{\uparrow\downarrow} / G_{\mathrm{NM}}\right) = \theta_{\mathrm{SH}}(2G_{\mathrm{eff}}^{\uparrow\downarrow} / G_{\mathrm{NM}}) \equiv \theta_{\mathrm{SH}} T_{\mathrm{int}}, \quad (2)$$

where $G_{\mathrm{eff}}^{\uparrow\downarrow} \equiv G^{\uparrow\downarrow} / (1 + 2G^{\uparrow\downarrow} / G_{\mathrm{NM}})$ is the effective spin mixing conductance and $T_{\mathrm{int}} \equiv 2G_{\mathrm{eff}}^{\uparrow\downarrow} / G_{\mathrm{NM}}$ describes the interfacial spin transparency. Values of $G_{\mathrm{eff}}^{\uparrow\downarrow}$ for the Pt/permalloy (Py) interface have been reported recently ranging from $G_{\mathrm{eff}}^{\uparrow\downarrow} = 0.6\times10^{15}\,\Omega^{-1}\mathrm{m}^{-2}$ to $1.2\times10^{15}\,\Omega^{-1}\mathrm{m}^{-2}$ [26, 31-33]. If we use previously-determined parameter values: $\xi_{DL} \approx 0.07$ (for $d_{\mathrm{Pt}} >> \lambda_{\mathrm{s,Pt}}$), $\lambda_{\mathrm{s,Pt}} \approx 1.4$ nm [3], and $\sigma_{\mathrm{Pt}} \approx 5\times10^{6}\,\Omega^{-1}\mathrm{m}^{-1}$ [3], Eqn. (2) indicates that the interfacial spin transparency is in the range between $T_{\mathrm{int}} \approx 0.34$ to $T_{\mathrm{int}} \approx 0.67$ and the internal spin Hall angle of Pt is between $0.10 \le \theta_{\mathrm{SH}} \le 0.20$, which is of course a substantial range of variation.

If there is a significant interfacial region "I" between the NM and FM layers where there is strong spin scattering, then Eqns. (1) and (2) do not provide an accurate description of the spin current flow. If the interfacial region can be at least approximately modeled as a separate layer of thickness t_{I}, and if we make the assumption that the spin Hall effect occurs only in the bulk of the

NM, Eqn. (1) can be adapted (see supplementary material [34]) for two normal metal layers (assuming $\mathrm{Re}\,G^{\uparrow\downarrow} >> \mathrm{Im}\,G^{\uparrow\downarrow}$),

$$\xi_{DL} = \theta_{\mathrm{SH}} \frac{\left[\cosh\left(d_{\mathrm{NM}} / \lambda_{\mathrm{s,NM}}\right) - 1\right]}{G_{\mathrm{I}} \cosh\left(d_{\mathrm{NM}} / \lambda_{\mathrm{s,NM}}\right)\sinh\left(t_{\mathrm{I}} / \lambda_{\mathrm{s,I}}\right) + G_{\mathrm{NM}} \cosh\left(t_{\mathrm{I}} / \lambda_{\mathrm{s,I}}\right)\sinh\left(d_{\mathrm{NM}} / \lambda_{\mathrm{s,NM}}\right)} \frac{2G^{\uparrow\downarrow}}{\left(1 + 2G^{\uparrow\downarrow} / G'_{\mathrm{ext}}\right)}. \tag{3}$$

Here $\lambda_{\mathrm{s,I}}$ is the spin diffusion length in the interfacial layer and G'_{ext} is the combined spin conductance of the two metal layers, given as [35] (note that there is a factor of two difference between here and Ref. [30] in the definition of G_{ext}):

$$G'_{\mathrm{ext}} = G_{\mathrm{I}} \left[\frac{G_{\mathrm{I}} \coth\left(d_{\mathrm{NM}} / \lambda_{\mathrm{s,NM}}\right) + G_{\mathrm{NM}} \coth\left(t_{\mathrm{I}} / \lambda_{\mathrm{s,I}}\right)}{G_{\mathrm{I}} \coth\left(d_{\mathrm{NM}} / \lambda_{\mathrm{s,NM}}\right)\coth\left(t_{\mathrm{I}} / \lambda_{\mathrm{s,I}}\right) + G_{\mathrm{NM}}} \right]. \tag{4}$$

Since in general it is not possible to measure t_{I} and $\lambda_{\mathrm{s,I}}$ directly, the spin flip parameter $\delta \equiv t_{\mathrm{I}} / \lambda_{\mathrm{s,I}}$ is used to quantify SML in multilayer NM|FM systems. In the limit where $d_{\mathrm{NM}} >> \lambda_{\mathrm{s,NM}}$ Eqn. (3) simplifies to

$$\xi_{DL} = \theta_{\mathrm{SH}} \frac{1}{\left(G_{\mathrm{NM}} / G_{\mathrm{I}}\right)\sinh(\delta) + \cosh(\delta)} \frac{2G^{\uparrow\downarrow}}{\left(G'_{\mathrm{ext}} + 2G^{\uparrow\downarrow}\right)}. \tag{5a}$$

Alternatively we can write this as

$$\xi_{DL} = \theta_{\mathrm{SH}} \frac{1}{G_{\mathrm{I}} \sinh(\delta) + G_{\mathrm{NM}} \cosh(\delta)} 2G'^{\uparrow\downarrow}_{\mathrm{eff}}, \tag{5b}$$

where $G'^{\uparrow\downarrow}_{\mathrm{eff}} \equiv G^{\uparrow\downarrow} / \left(1 + 2G^{\uparrow\downarrow} / G'_{\mathrm{ext}}\right)$. A value of $\delta = 0.9$ has recently been reported for the SML of sputter-deposited Pt/Co multilayers from a low temperature giant magnetoresistance study [36]. If such a strong SML is present in a Pt/FM bilayer system where the anti-damping spin torque efficiency has been measured to be $\xi_{DL} \approx 0.07$ then again this indicates that the internal spin Hall

ratio of Pt can be quite high, with the exact value indicated by this value of ξ_{DL} depending on the spin conductances of the two normal metal layers, G_{I} and $G_{\mathrm{NM(Pt)}}$.

Here we report quantitative measurements of the damping-like and field-like torques exerted by the SHE-generated spin currents acting on thin Co and CoFe layers placed in contact with Pt thin film microstrips. We have studied both perpendicularly-magnetized (PM) structures and in-plane magnetized (IPM) structures, measuring the spin-torque efficiencies by the harmonic response technique [4, 5, 37] (PM cases) and by spin-torque ferromagnetic resonance (ST-FMR) [7] (IPM cases). We observed variations in the spin torque efficiencies that depend on the magnetic properties and thickness of the FM layer, and on post-growth thermal processing protocols. Depending on the choice of the FM and the nature of the interface, we find that ξ_{DL} for the Pt/FM system can vary from < 0.05 to > 0.10, with the latter results substantially enhancing the potential value of Pt for three-terminal spin Hall device applications see e.g. [27], [38], and [39]. We also find that the measurement of the FMR linewidth as a function of the FM thickness of the samples studied here gives results for the apparent effective spin mixing conductance of the interface that are quite variable, and in some cases unphysical. This can make determination of the spin transparency of the Pt/FM interface from spin pumping measurements problematic. However in some cases $G_{\mathrm{eff}}^{\uparrow\downarrow}$ is reasonably close to theoretical predictions and then the combined measurement of ξ_{DL} and $G_{\mathrm{eff}}^{\uparrow\downarrow}$ indicates that the internal spin Hall ratio of Pt is between 0.2 and 0.3.

Sample preparation

Since there appears to be considerable variation in the spin torque efficiency reported in the literature recently for similar Pt/FM systems [20-25] the details of the deposition process may be

important. The multilayer films for this investigation were produced by direct current (DC) sputtering (RF magnetron for the insulating layers) from 2-inch planar magnetron sources onto thermally-oxidized Si substrates in a vacuum system with a base pressure $< 4\times10^{-8}$ Torr. The target to substrate separation was approximately 18 cm. This separation together with an oblique orientation of the target to the substrate resulted in a low deposition rate of ≈ 0.01 nm/s (Ta: 0.0135 nm/s, Pt: 0.017 nm/s, Co: 0.0064nm/s, CoFe: 0.0092 nm/s) with DC sputtering conditions of 2 mTorr Ar and 30 watts power. We prepared six series of samples: (A) ||Ta(2)/Pt(4)/Co(t_{Co})/MgO(2)/Ta(1) with $0.5 \text{ nm} \le t_{Co} \le 1.3 \text{ nm}$, (B) ||Ta(2)/Pt(4)/$Co_{50}Fe_{50}$($t_{CoFe}$)/MgO(2)/Ta(1) with $0.4 \text{ nm} \le t_{CoFe} \le 1.1 \text{ nm}$ and with the samples vacuum annealed at 350°C for 30 minutes, (C) ||$Co_{50}Fe_{50}$(t_{CoFe})/Pt(4) with $1 \text{ nm} \le t_{CoFe} \le 9 \text{ nm}$, (D) ||$Co_{50}Fe_{50}$($t_{CoFe}$)/Pt(4) with $1 \text{ nm} \le t_{CoFe} \le 9 \text{ nm}$ and with the samples vacuum annealed at 350°C for 30 minutes, (E) ||Ta(2)/Pt(4)/Co(t_{Co})/MgO(2)/Ta(1) with $2 \text{ nm} \le t_{Co} \le 9 \text{ nm}$ and (F) ||MgO(1.6)/Co(t_{Co})/Pt(4) with $2 \text{ nm} \le t_{Co} \le 9 \text{ nm}$. The numbers in the parentheses represent the nominal thicknesses of the sputtered films, in nm, and || represents the oxidized Si substrate. The Ta base layer in series (A), (B) and (E) was employed as a seeding and smoothing layer, as we have found that it results in much stronger perpendicular magnetic anisotropy (PMA) than exhibited by Pt/Co layers deposited without the Ta seed layer. The as-deposited series (A) showed strong PMA without any further annealing for $0.6 \text{ nm} \le t_{Co} \le 1.3 \text{ nm}$. Series (B) required an annealing temperature of 350°C for 1 hour to obtain PMA, for $0.5 \text{ nm} \le t_{CoFe} \le 0.7 \text{ nm}$. Series (C), (D), (E) and (F) all exhibited in-plane magnetic anisotropy over their entire thickness range, but with some significant differences in the variation of

the strength of the demagnetization field with thickness between these series, as we will discuss further below. The specifications of the different series of samples are listed in Table I.

Magnetic properties and spin torque efficiencies of PM Pt/FM series

The magnetic properties of our sputtered Co and CoFe films in series (A) and (B) are summarized in Fig. 1. We measured the FM layer thickness dependence of the magnetization by superconducting quantum interference device (SQUID) magnetometry. As shown in Fig. 1(a), the as-deposited Co (series (A)) has a saturation magnetization $M_s = 1084 \pm 50$ emu/cm^3 and an apparent magnetic dead layer thickness of $t_D = 0.26 \pm 0.04$ nm as estimated from the slope and the intercept of the linear fit, respectively. Such dead layers may arise from some intermixing of the FM and normal metal layers [40] and/or from some oxidation of FM surface during the deposition of the oxide layer [41]. We also measured the temperature (T) dependence of magnetization for $t_{\mathrm{Co}} = 1$ nm sample, which is shown in Fig. 1(b). Although the magnetization of Co increases while decreasing temperature from 300 K to 100 K, the variation is less than 10%, consistent with behavior expected of a smooth, three-dimensional magnetic system with a high Curie temperature. As shown in Fig. 1(c), for the thin as-deposited CoFe films (series (B)) we found $M_s = 1720 \pm 70$ emu/cm^3 and no apparent magnetic dead layer. However, an apparent magnetic dead layer of $t_D = 0.34 \pm 0.02$ nm is formed after the annealing process, and the *apparent* saturation magnetization (from the slope of the linear fit) increases to $M_s = 2884 \pm 60$ emu/cm^3, though the *de facto* total magnetic moment decreases. The temperature dependence of the magnetic moment of the annealed CoFe layers is also significantly different from that of the Co case, with the moment increasing strongly upon cooling to low temperature. For example, as shown in Fig. 1(d) the moment per unit area of the $t_{\mathrm{CoFe}} = 0.6$ nm

film increases by ~ 50% upon cooling from 300 K to 100 K. This corresponds to a quite reasonable low T saturation magnetization $M_s \approx 1800$ emu/cm^3 if we assume an effective thickness of 0.6 nm. This suggests the absence of a significant dead layer at low T and seems to support the possibility that the room temperature dead layer is due to intermixing of the Pt and CoFe.

We also characterized the magnetic anisotropy energy density K_{eff} in both the as-deposited Co series (A) and annealed CoFe series (B) samples [42], as summarized in Fig. 1(e) and (f). We performed linear fits to $K_{\text{eff}} t_{FM}^{\text{eff}}$ vs. t_{FM}^{eff} (with $t_{FM}^{\text{eff}} = t_{FM} - t_D$) in the large-thickness linear regime, which corresponds to the regime of relaxed lattice strain in the FM layer [43], to estimate the interfacial anisotropy energy K_s from the intercept: $K_s = 1.10 \pm 0.13$ erg/cm^2 for Co series (A) and $K_s = 0.88 \pm 0.15$ erg/cm^2 for annealed CoFe series (B).

To evaluate ξ_{DL} and ξ_{FL} for the PMA samples, series (A) and (B), we patterned those thin films into micrometer-sized Hall-bar structures, and measured the harmonic response (HR) of the anomalous Hall voltage of these samples to a low frequency (≈10Hz) alternating current passed through the bilayer to determine the effective anti-damping and field-like torques τ_{DL} and τ_{FL}, or equivalently the longitudinal and transverse effective fields ($H_L \propto \xi_{DL} J_e (\hat{\sigma} \times \hat{m})$ and $H_T \propto \xi_{FL} J_e \hat{\sigma}$) exerted on the perpendicular magnetization [4, 5, 37]. From this and the measured saturation magnetization $M_s(T)$ of Co and CoFe, the (temperature dependent) spin torque efficiencies, $\xi_{DL}(T)$ and $\xi_{FL}(T)$, can be obtained by (modified from Khvalkovskiy *et al*. [44])

$$\xi_{DL(FL)}(T) = \left(\frac{2e}{\hbar}\right) 4\pi M_s(T) t_{FM}^{\text{eff}} \left(\frac{H_{L(T)}}{J_e}\right). \quad (6)$$

In Fig. 2(a) we show both the damping-like and field-like spin-torque efficiencies at room temperature as determined by HR measurements and Eqn. (6) for the series (A) Pt/Co/MgO samples. The former increases from $\xi_{DL} \approx 0.01$ to $\xi_{DL} \approx 0.12$ as the Co thickness increases from 0.6 nm to 0.9 nm. The latter, although considerably smaller, shows a similar behavior, increasing from $\xi_{FL} \approx 0.00$ for $t_{\mathrm{Co}} = 0.6$ nm to $\xi_{FL} \approx 0.03$ at the thick Co limit, $t_{\mathrm{Co}} \geq 1.0$ nm. The maximum value for ξ_{DL} that we have obtained here is approximately double, or more, compared to the values reported by early ST-FMR on samples with much thicker Py layers (≥ 4 nm) [3, 7] and also by inverse spin Hall effect (ISHE)-spin pumping measurements of comparatively thick IPM Pt/Py bilayers [45, 46]. This value $\xi_{DL} \approx 0.12$ is also larger than that obtained from PM Pt/CoFe (0.6 nm)/MgO structures using the same HR technique ($\xi_{DL} \approx 0.06$) [47] and from magnetic reversal studies on annealed PM Pt/Co/MgO layers formed without a templating Ta seed layer ($\xi_{DL} \approx 0.07$) [48]. However recent ISHE studies of IPM Pt/Py and Pt/YIG have respectively reported $\xi_{DL} \approx 0.12$ [23] and $\xi_{DL} \approx 0.10$ [22], and an even higher value $\xi_{DL} = 0.16$ was found recently for Pt/Co/AlO_x from HR measurements in the PM case [5]. Using ST-FMR measurements on in-plane magnetized samples, Zhang *et al.* also estimated $\xi_{DL} \approx 0.11$ for Pt/Co bilayer structures [26].

In seeking an explanation for the variation of ξ_{DL} (and ξ_{FL}) with t_{Co} in the series (A) samples, we speculate that it may be necessary for the Co film to reach a critical magnetic thickness, ~ 0.6 nm, to attain the full spin transfer torque [49], and the 0.26 nm magnetic dead layer could be playing a role, as well. However, it is also interesting to note that sputter-deposited Ta(seed)/$(Pt/Co)_n$ multilayers have been reported to be structurally coherent, with a (111) normal texture in the ultra-thin Co limit, but when the Co becomes thicker than ~ 1 nm the elastic strain due to the ~ 10% lattice mismatch can no longer be supported and the interface relaxes via the formation of misfit

dislocations, and the Co and Pt layers become incoherent [43]. The magnetic anisotropy behavior of our sputtered Ta(seed)/Pt/Co/MgO heterostructures is consistent with that of Ref [43] where a thickness-dependent magnetoelastic effect associated with interfacial strain (See Fig. 1(e)) reflects this transition from a strained to a relaxed Co layer. Thus the increase we observe for both ξ_{DL} and ξ_{FL} as a function of increasing t_{Co} might therefore be related, at least in part, to the transition from a strained and coherent (111) Pt/Co interface to a relaxed and incoherent (111) one. Given Eqn. (1), our results also suggest that the increase in the $\xi_{DL(FL)}$ with Co thickness could be associated with an increase in $G^{\uparrow\downarrow}$ relative to G_{Pt} as the Pt/Co interface transitions from a highly strained, coherent (111) interface to a relaxed, incoherent (111) interface, although to our knowledge a calculation of $G^{\uparrow\downarrow}$ for such Pt/Co interfaces has not yet been reported.

To further examine how the character of the Pt/FM interface can change the behavior of ξ_{DL} and ξ_{FL} for systems with PMA, we also performed HR measurements on the annealed Pt/CoFe/MgO series (B) samples. The resulting ξ_{DL} and ξ_{FL} are shown in Fig. 3(a) as a function of the CoFe thickness t_{CoFe}. The first distinct difference compared to the Pt/Co/MgO case is that the magnitude of ξ_{DL} and ξ_{FL} are both high, ≈ 0.15 for the thinnest layers, t_{CoFe} = 0.5 nm, but they *decrease* as a function of increasing t_{CoFe}, with ξ_{FL} decreasing more rapidly. A second difference is that the sign of ξ_{FL} is now reversed, negative in our convention, opposing the Oersted field generated by current flow in the Pt. While both the as-deposited Pt/Co and annealed Pt/CoFe PM samples exhibit an apparent magnetic dead layer (0.26 nm and 0.34 nm respectively), X-ray diffraction studies on Pt/Co and Pt/CoFe bi-layers where for signal to noise purposes the FM layers are somewhat thicker, ≥ 2 nm) indicate a significant difference between the two systems: The as-deposited Pt/Co bilayer exhibits

only (111) texture, while the annealed Pt/CoFe bilayer shows both a Pt (111) normal texture as well as a (110) component that we attribute to the CoFe [34]. Therefore for the annealed series (B) samples we have a Pt (111)/CoFe (110) interface, unlike the as-deposited series (A) that possesses a Pt(111)/Co(111) interface. Also, as we discuss in the following section, spin torque and damping measurements on thicker IPM Pt/CoFe samples that also have been annealed, series (D), indicate the presence of some significant spin memory loss at the interface of the annealed samples, presumably due to intermixing driven by the annealing process. Perhaps the degree of this intermixing depends, in the limit of a thin CoFe layer, on its thickness.

While the temperature dependence of the spin-orbit torques of these PMA samples is not the main focus of this report, that behavior does reveal a third difference between the spin torque behavior of the unannealed Pt/Co PMA series (A) and that of the annealed Pt/CoFe PMA series (B). We performed HR measurements as a function of T on one of the samples from series (A), namely Ta(2)/Pt(4)/Co(1)/MgO(2)/Ta(1). As shown in Fig. 2(b), no significant T-dependence was found for either component of torque down to $T = 50\,\mathrm{K}$. This is strikingly different from the annealed Pt/CoFe PMA samples in series (B). Fig. 3(b) shows the corresponding results for a Pt(4)/CoFe(0.6)/MgO(2)/Ta(1) sample; both components of spin torque efficiency vary quasi-linearly with temperature down to $T \approx 50$ K and then more slowly reach their limiting values at ≈ 25 K. The variation of ξ_{FL} is far stronger than that of ξ_{DL}, so that ξ_{FL} becomes essentially zero by T = 25 K whereas $\xi_{DL} \approx 0.07$ in the low T regime. Previous studies have reported a wide range of behaviors for the temperature dependence for the spin torque efficiency in Pt/FM samples. Previous experiments on the Ta/CoFeB/MgO system [50, 51] found results qualitatively similar to our series (B) devices, with a field-like component even stronger than ours (at T = 300 K) and possessing a strong T dependence, while the T dependence of the damping-like component was weaker, but still

significant. On the other hand spin Hall magnetoresistance measurements of Pt/YIG bilayer samples [21] have indicated a value $\xi_{DL} \approx 0.10$ that is approximately independent of T for $T \geq 100\,\mathrm{K}$, much like our series (A) samples, although this agreement may be fortuitous since the interfacial electronic structure for Pt/YIG is certainly quite different from that of Pt/Co although the spin mixing conductance has been reported to be similar for a wide variety of Pt/FM interfaces [25].

These differences clearly indicate that the nature of spin transport at the annealed Pt/CoFe interface (series (B)) is significantly different from that of the as-deposited Pt/Co interface (series (A)). Our finding that ξ_{FL} is comparable to ξ_{DL} in the annealed Pt/CoFe case is of course not immediately consistent with a SHE origin for both spin torque components since calculations find that $\mathrm{Re}G^{\uparrow\downarrow} >> \mathrm{Im}G^{\uparrow\downarrow}$ for NM/FM interfaces, even when some disorder is included [30], unless for some reason a disordered interface requires a thicker FM to reach the expected $\mathrm{Re}G^{\uparrow\downarrow} >> \mathrm{Im}G^{\uparrow\downarrow}$ regime. However it is also not yet clear how either a Rashba-like effect at the NM/FM or FM/Oxide interface [11, 52], or the SHE, can provide a mechanism to explain the strong T dependence of τ_{FL} for what is most likely a disordered Pt/CoFe interface.

Magnetic properties and spin torque efficiencies of IPM Pt/FM series

In Fig. 4 we summarize the magnetization properties of the thick, IPM CoFe/Pt series (C) and series (D), and the thick IPM Co series (E) and series (F) samples. Fig. 4(a) shows the FM layer thickness dependence of the magnetization of the as-deposited CoFe/Pt series (C) and the annealed CoFe/Pt series (D) samples, where here the data were taken by vibrating sample magnetometry (VSM). The linear fit to the series (C) data yields t_D = 0.30 ± 0.10 nm and M_s = 1560 ± 40 emu/cm^3. For series (D), the annealed samples, a much thicker magnetic dead layer was found, with t_D = 0.70 ± 0.10 nm and M_s = 1820 ± 40 emu/cm^3. The increase of the magnetic dead layer thickness as well

as the saturation magnetization after the annealing process is similar to the trend found in the thinner CoFe case (series (B)). We determined the effective demagnetization field $4\pi M_{\text{eff}}$ of the series (C) and series (D) samples via the Kittel formula from the spin torque ferromagnetic resonance (ST-FMR) frequency. From this we calculated the effective magnetic anisotropy energy density of the as-deposited (C) and annealed CoFe/Pt samples (D) and plot the results in Fig. 4(b) in terms of $K_{\text{eff}} t_{\text{CoFe}}^{\text{eff}}$ as a function of $t_{\text{CoFe}}^{\text{eff}}$. The plot indicates that the interfacial anisotropy energy density of the IPM as-deposited CoFe/Pt films, as estimated from the intercept of the linear fit [42], is $K_s^{\text{as-deposited}} = 0.48 \pm 0.17$ erg/cm^2. After annealing and the increase of the apparent dead layer this anisotropy slightly increases to $K_s^{\text{annealed}} = 0.52 \pm 0.21$ erg/cm^2. The change of the slope for linear fits in Fig. 4(b) corresponds to the change of saturation magnetization term, i.e., $-2\pi M_s^2$ [42], after annealing. For reference, the results from the annealed Pt/CoFe/MgO series (B) samples with perpendicular magnetic anisotropy, as determined by SQUID magnetometry are also plotted on the same figure, which indicate a small enhancement of K_s with the addition of the CoFe/MgO interface. We show the FM layer thickness dependence of the magnetization of the Pt/Co/MgO series (E) and the MgO/Co/Pt series (F) samples in Fig. 4(c), again as determined by VSM. The linear fit to the series (E) data yields t_D = 0.39 ± 0.09 nm and M_s = 1290 ± 20 emu/cm^3. For the Co films grown on a MgO seed layer, the data indicate a slightly thicker dead layer, t_D = 0.5 ± 0.2 nm, and slightly lower M_s = 1270 ± 30 emu/cm^3. Finally in Fig. 4(d) we plot $K_{\text{eff}} t_{\text{Co}}^{\text{eff}}$ vs. $t_{\text{Co}}^{\text{eff}}$ as determined from ST-FMR measurement of the Pt/Co/MgO series (E) films and of the MgO/Co/Pt series (F) films. The much higher value of the interfacial anisotropy energy that we observed when the Co is deposited on top of the Pt (series (E)), than in the opposite case (series (F)), $K_s^{\text{Pt/Co}} = 1.70 \pm 0.07$ erg/cm^2 vs. $K_s^{\text{Co/Pt}} = 0.84 \pm 0.10$ erg/cm^2 suggests a considerably different Pt/Co interface in the two different

series, consistent with previous work [53].

Since the HR measurements are mainly suitable for devices with PMA, to further examine the modifications that can occur in interfacial spin transport due to changes in the details of the Pt/FM interface in the thicker FM regime ($t_{FM} \geq 1\,\mathrm{nm}$), we carried out ST-FMR measurements on micrometer-sized bar-like structures patterned out of series (C) and (D) IPM CoFe/Pt samples, and series (E) and series (F) IPM Pt/Co samples. In the former case we studied samples with and without annealing at 350°C.

In our research group's first paper on ST-FMR using samples with thick (≥4 nm) Py layers [7], we utilized a so-called self-calibrated analysis in which we assumed that the only contribution to ξ_{FL} comes from the current-induced Oersted field. In this case the amplitude of the antisymmetric component (*A*) ST-FMR resonance can be used to calibrate the current density in the NM, and ξ_{DL} can then be related in a simple way to the ratio *S/A*, where *S* is the amplitude of the symmetric component of the resonance. However, it is now understood that in some HM/FM samples there can exist a significant spin-orbit-induced field-like torque τ_{FL} in addition to the Oersted-field τ_{Oe} so that this self-calibrated analysis fails, giving a false impression that the anti-damping spin-torque efficiency depends strongly on the FM layer thickness [15, 54]. One way to correct the analysis is through a separate calibration of the microwave current in the sample using a network analyzer [55]. Here we introduce an even simpler approach: measuring the dependence of the ST-FMR amplitude ratio *S/A* on the FM layer thickness and using an analysis which takes into account explicitly the possibility of a spin-orbit-generated contribution to ξ_{FL} (in addition to the Oersted field). Specifically, we analyze the quantity ξ_{FMR}, defined from the ST-FMR *S/A* ratio as

$$\xi_{FMR} = \frac{S}{A}\left(\frac{e}{\hbar}\right) 4\pi M_s t_{FM}^{\mathrm{eff}} d_{NM} \sqrt{1+\left(4\pi M_{\mathrm{eff}} / H_0\right)} \ . \qquad (7)$$

The relative amplitudes of the symmetric and antisymmetric components of the ST-FMR resonance can be related to the underlying spin-orbit and Oersted-field torques according to (modified from Liu et al. [7])

$$S = \frac{\hbar}{2e}\frac{\xi_{DL} J_e^{rf}}{4\pi M_s t_{FM}^{\text{eff}}} \text{ and} \tag{8}$$

$$A = \left(H_T + H_{Oe}\right)\sqrt{1+\left(4\pi M_{\text{eff}} / H_0\right)} = \left(\frac{\hbar}{2e}\frac{\xi_{FL} J_e^{rf}}{4\pi M_s t_{FM}^{\text{eff}}} + \frac{J_e^{rf} d_{NM}}{2}\right)\sqrt{1+\left(4\pi M_{\text{eff}} / H_0\right)}. \tag{9}$$

Here t_{FM}^{eff}, d_{NM}, $4\pi M_{\text{eff}}$, H_0, J_e^{rf}, $H_T \propto \tau_{FL}$, and $H_{Oe} \propto \tau_{Oe}$ represent the effective thickness of FM layer, the thickness of NM layer, the effective demagnetization field of the FM layer, the ferromagnetic resonance field, the RF charge current density in the NM layer, the RF effective field (from the RF current-induced field-like torque τ_{FL}) and the RF Oersted field, respectively. H_0 is the magnitude of the external magnetic field applied in-plane. For samples with $\tau_{FL} << \tau_{Oe}$ ($i.e., H_T << H_{Oe}$), ξ_{FMR} should be independent of t_{FM}^{eff} and one will have $\xi_{FMR} = \xi_{DL}$. However, when τ_{FL} is significant compared to τ_{Oe}, then ξ_{FMR} will depend on t_{FM}^{eff} (since $H_T \propto \xi_{FL} / t_{FM}^{\text{eff}}$ while H_{Oe} is independent of t_{FM}^{eff}), and ξ_{FMR} will then differ from ξ_{DL}. In general, this thickness dependence should be most significant for thin ferromagnetic layers, ≤ 2-3 nm. Rearranging Eqns. (7)-(9), we expect

$$\frac{1}{\xi_{FMR}} = \frac{1}{\xi_{DL}}\left(1 + \frac{\hbar}{e}\frac{\xi_{FL}}{4\pi M_s t_{FM}^{\text{eff}} d_{NM}}\right). \tag{10}$$

Under the assumption that the values of ξ_{DL} and ξ_{FL} do not depend strongly on t_{FM} for FM layers thicker than 1 nm (which provides good fits in most, but not all cases), ξ_{DL} and ξ_{FL} can then be determined by comparing the measured dependence of ξ_{FMR} on t_{FM} to Eqn. (10).

For our *as-deposited* CoFe/Pt bilayers (C), this ST-FMR analysis yields $\xi_{FMR} \approx 0.10$ with no significant t_{CoFe} dependency for $1\ \mathrm{nm} \le t_{\mathrm{CoFe}} \le 7\ \mathrm{nm}$ (Fig. 5(a)), indicating that τ_{FL} is negligible in these as-deposited samples. On the other hand, ξ_{FMR} of the *annealed* IPM Pt/CoFe bilayers (D) exhibits a sign change at $t_{\mathrm{CoFe}} \approx 1.5\ \mathrm{nm}$ (associated with a sign change in the anti-symmetric component of the ST-FMR signal), consistent with the presence of both a field-like spin-orbit torque and an Oersted torque with opposite signs and changing relative magnitudes. Performing a linear fit to $1/\xi_{FMR}$ vs. $1/t_{\mathrm{CoFe}}^{\mathrm{eff}}$, where $t_{\mathrm{CoFe}}^{\mathrm{eff}}$ represents an effective thickness of CoFe layer excluding the thickness of the magnetic dead layer, and using Eqn. (10) we find $\xi_{DL}^{\text{as-deposited}} = 0.10 \pm 0.005$ and $\xi_{FL}^{\text{as-deposited}} = -0.004 \pm 0.002$, while $\xi_{DL}^{\text{annealed}} = 0.077 \pm 0.005$ and $\xi_{FL}^{\text{annealed}} = -0.011 \pm 0.003$. The substantial changes in ξ_{DL} and ξ_{FL} with annealing demonstrate the sensitivity of the interfacial spin transport to the details of the composition and processing of the NM/FM interface. As discussed below this may be related to the formation of a SML layer upon annealing.

In Fig. 5(c) we plot ξ_{FMR} as determined from ST-FMR for the series (E) Pt/Co/MgO samples as a function of t_{Co}, and also for the "inverted" series (F) MgO/Co/Pt samples. The thicker samples of series (E) show $\xi_{FMR} \approx 0.1$, similar to the as-deposited CoFe/Pt (series (C)) result while the $t_{\mathrm{Co}} = 2$ and 3 nm samples in series (E) have an even higher $\xi_{FMR} \approx 0.18$. This could be indicating the presence of a significant field-like torque for the two thinner Co layers, or possibly there is some

interfacial structure change in the thin film limit that results in an enhanced ξ_{DL}, but more work will be required to confirm that. The series (F) samples exhibit a ξ_{FMR} with a substantial variation at small t_{Co} that is characteristic of the presence of a strong field-like torque. A linear fit to a plot of $1/\xi_{FMR}$ against $1/t_{\mathrm{Co}}^{\mathrm{eff}}$ for the thinner samples from this series (See Fig. 5(d)) indicates that $\xi_{DL}^{\mathrm{Pt/Co/MgO}} = 0.064 \pm 0.005$ and $\xi_{FL}^{\mathrm{Pt/Co/MgO}} = -0.029 \pm 0.001$.

Inspection of Fig. 5(d) reveals that for the Pt/Co/MgO series (E) samples the anti-damping spin-torque efficiency appears to decrease once $t_{\mathrm{Co}} > 5$ nm. We do not have a satisfactory explanation for this behavior but we do note that X-ray diffraction [34] indicates that the crystalline orientation of the Co transitions from a (111) normal orientation for the thinner layers, the same as that of the Pt layer, to having a significant component with the (110) orientation once the Co thickness exceeds 5 nm. Perhaps the change in crystal orientation is a cause for a reduction in ξ_{DL} in the thick limit. For our MgO/Co/Pt series (F) films the X-ray spectra predominately exhibit the (111) peak at $\approx 40^{\circ}$, with this peak being much broader than for the series (E) films. This may be indicative of thickness dependent strain in the textured films grown on MgO in comparison to the Co films grown on Pt. In the series (F) film there is only a weak signal indicative of some small (110) Co grains, and only in the thicker samples.

Magnetic damping and spin-pumping analysis

The harmonic response behavior of the PM samples and ST-FMR results from the IPM samples demonstrate that the anti-damping spin torque efficiency of Pt/FM systems is variable, but it can be rather high in some cases, $\xi_{DL} \geq 0.10$, consistent with other recent reports [5, 23, 26, 27]. This raises the question as to what is the internal spin Hall ratio of sputter-deposited Pt thin films and, if

high, as to whether the spin transparency of Pt/FM interfaces can be enhanced to take greater advantage of this for spin torque applications. We can attempt to examine the question by determining the effective spin-mixing conductance and hence the spin transparency for the different the IPM Pt/FM samples by analyzing the effective magnetic damping constant α, as calculated from the variation of the linewidth of the ST-FMR signals as a function of applied field [7]. As is the case for the ST-FMR determination of the spin torque efficiencies, the damping results are also rather variable between the different IPM series.

In Fig. 6(a) we show α for both the as-deposited and annealed CoFe/Pt, series (C) and series (D) samples. In both cases α increases with decreasing t_{CoFe}, but the increase is much more pronounced for the annealed samples, with the thinnest annealed CoFe sample having a damping constant about five times larger than its as-deposited counterpart. According to the theory of spin pumping, the enhancement of α with the placement of a NM next to FM layer can, in the absence of significant SML, be related to the effective spin-mixing conductance [56, 57]

$$g_{\mathrm{eff}}^{\uparrow\downarrow} = \frac{4\pi M_s t_{FM}^{\mathrm{eff}}}{\gamma\hbar}\left(\alpha - \alpha_0\right) = \frac{4\pi M_s t_{FM}^{\mathrm{eff}}}{\gamma\hbar}\Delta\alpha, \tag{11}$$

where $g_{\mathrm{eff}}^{\uparrow\downarrow} \equiv G_{\mathrm{eff}}^{\uparrow\downarrow}(h/e^2)$ and M_s, t_{FM}^{eff}, α_0, and $\gamma = 1.76\times10^{11}\,\mathrm{s^{-1}T^{-1}}$ represent the saturation magnetization, the effective thickness, the intrinsic damping constant, and the gyromagnetic ratio of the FM layer, respectively. (We note that the assumption of the free electron value for γ introduces some error, ≤ 5%, into the results of the analysis here, but this does not have a significant impact on the conclusions presented below.) By plotting α against $1/t_{\mathrm{CoFe}}^{\mathrm{eff}}$, as shown in Fig. 6(b), and performing linear fits based on Eqn. (11), we obtain $g_{\mathrm{eff,\,as\text{-}deposited}}^{\uparrow\downarrow} = (9.8\pm0.2)\times10^{18}\,\mathrm{m^{-2}}$ and

$\alpha_0 = 0.009 \pm 0.001$ for our as-deposited CoFe/Pt series (C). This value of $g_{\text{eff}}^{\uparrow\downarrow}$ is at the low end of the range of values reported previously for Pt/Co interfaces [58, 59]. In the limit of $\text{Re}\,G^{\uparrow\downarrow} >> \text{Im}\,G^{\uparrow\downarrow}$, the bare spin-mixing conductance $G^{\uparrow\downarrow}$ can be further calculated from $g_{\text{eff}}^{\uparrow\downarrow}$ by taking the spin back flow at the NM/FM interface into account, with [57]

$$G^{\uparrow\downarrow} = \frac{\dfrac{\sigma_{\text{Pt}}}{2\lambda_{\text{s,Pt}}}\left(\dfrac{e^2}{h}\right) g_{\text{eff}}^{\uparrow\downarrow}}{\dfrac{\sigma_{\text{Pt}}}{2\lambda_{\text{s,Pt}}} - \left(\dfrac{e^2}{h}\right) g_{\text{eff}}^{\uparrow\downarrow} \coth\left(\dfrac{d_{\text{Pt}}}{\lambda_{\text{s,Pt}}}\right)} = \frac{G_{\text{eff}}^{\uparrow\downarrow}}{1 - 2G_{\text{eff}}^{\uparrow\downarrow} / G_{\text{Pt}}}. \qquad (12)$$

Using $d_{\text{Pt}} = 4\text{nm}$, $\lambda_{s,\text{Pt}} \approx 1.4\,\text{nm}$ [3] and the measured Pt conductivity $\sigma_{\text{Pt}} = 3.2 \times 10^6\ \Omega^{-1}\text{m}^{-1}$, we find that $G_{\text{as-deposited}}^{\uparrow\downarrow} = (0.57 \pm 0.02) \times 10^{15}\ \Omega^{-1}\text{m}^{-2}$. This result for the spin mixing conductance is comparable to the result of a model calculation $G^{\uparrow\downarrow} = 0.59 \times 10^{15}\ \Omega^{-1}\text{m}^{-2}$ for the Co/Pt interface [13] and a first-principals calculation of the Sharvin conductance of Pt $G_{Sh} = 0.68 \times 10^{15}\ \Omega^{-1}\text{m}^{-2}$ [60, 61]. We can then estimate the internal spin Hall angle of Pt $\theta_{\text{SH}}^{\text{Pt}}$ with Eqn. (1) by using this $G_{\text{as-deposited}}^{\uparrow\downarrow}$ and the measured $\xi_{DL}^{\text{as-deposited}}$ (since $|\xi_{DL}| >> |\xi_{FL}|$ in the as-deposited case this implies that for these samples we indeed have $\text{Re}\,G^{\uparrow\downarrow} >> \text{Im}\,G^{\uparrow\downarrow}$). This yields $\theta_{\text{SH}}^{\text{Pt}} = 0.33 \pm 0.05$, which is larger than but still comparable to the estimation from previous Pt/Py results. We note that the estimated thickness of the magnetic dead layer t_D will affect the estimation of $\theta_{\text{SH}}^{\text{Pt}}$ to some degree. For instance, without the consideration of t_D in our as-deposited CoFe films the same analysis will yield $\theta_{\text{SH}}^{\text{Pt}} = 0.21 \pm 0.04$.

The situation is quite different for the annealed CoFe/Pt series (C) samples. As also shown in Fig 6(b), while in the limit of a very thick CoFe layer the annealed films have essentially the same intrinsic damping $\alpha_0 \approx 0.009$, the variation of damping with $1/t_{\text{CoFe}}^{\text{eff}}$ is much stronger in the annealed

case. A linear fit to the data indicates $g_{\text{eff, annealed}}^{\uparrow\downarrow} \approx 5.1\times10^{19}\,\text{m}^{-2}$ (or $G_{\text{eff}}^{\uparrow\downarrow} \approx 1.98\times10^{15}\,\Omega^{-1}\text{m}^{-2}$), about five times the value as for the as-deposited case. If we attempt to apply Eqn. (12) together with this value of $g_{\text{eff, annealed}}^{\uparrow\downarrow}$, the result is what appears to be an unphysical value for $G^{\uparrow\downarrow}$. This is because $G_{\text{eff}}^{\uparrow\downarrow} > G_{\text{Pt}}/2$ for $\sigma_{\text{Pt}} = 3.2\times10^{6}\,\Omega^{-1}\text{m}^{-1}$ with $\lambda_{s,\text{Pt}} = 1.4$ nm and thus $G^{\uparrow\downarrow} < 0$. If we assume a quite high electrical conductivity, $\sigma_{\text{Pt}} \approx 5.6\times10^{6}\,\Omega^{-1}\text{m}^{-1}$, in combination with a short spin diffusion length ≈ 1.4 nm, that could result in $G_{\text{eff}}^{\uparrow\downarrow} < G_{\text{Pt}}/2$ and hence a positive $G^{\uparrow\downarrow}$. However since one must have $G^{\uparrow\downarrow} \geq G_{\text{eff}}^{\uparrow\downarrow}$ in all cases for a drift diffusion analysis, this requires that $G^{\uparrow\downarrow} \geq 1.98\times10^{15}\,\Omega^{-1}\text{m}^{-2}$. This is considerably greater than expected from calculations [60, 61] and thus is, we conclude, essentially as unphysical as a negative value.

The two IPM sets of Co samples, Pt/Co/MgO series (E) and MgO/Co/Pt series (F), also exhibit enhanced damping nominally indicative of a quite high $g_{\text{eff}}^{\uparrow\downarrow}$, as shown in Fig. 6(c). In both cases a plot of α as a function of $1/t_{\text{Co}}^{\text{eff}}$ can be reasonably well fit by a straight line for the thicker samples, $t_{\text{Co}}^{\text{eff}} \geq 3$ nm (Fig. 6(d)), yielding $g_{\text{eff}}^{\uparrow\downarrow} \approx 5.1\times10^{19}\,\text{m}^{-2}$ for the series (E) samples and $g_{\text{eff}}^{\uparrow\downarrow} \approx 5.3\times10^{19}\,\text{m}^{-2}$ for series (F). These are again about five times the value as for the as-deposited series (C) samples. For $t_{\text{Co}}^{\text{eff}} < 3$ nm both series show an even more rapid increase in damping with $1/t_{\text{Co}}^{\text{eff}}$. Such enhanced damping in very thin Co layers has been reported previously [62]. We note that the increase is greater for the Pt/Co/MgO series (E), which is the one of the two series that has the stronger interfacial anisotropy energy density (see Fig. 4(d)) so this increase may be associated with that interface effect, or perhaps simply be a consequence of the reduced anisotropy. Finally we note that two recent studies of Pt/Co bilayer samples have also reported high spin-mixing

conductances, $g_{\text{eff}}^{\uparrow\downarrow} \approx 8\times10^{19}\,\text{m}^{-2}$ [17] and $g_{\text{eff}}^{\uparrow\downarrow} \approx 3.96\times10^{19}\,\text{m}^{-2}$ [26]. Again these values of $g_{\text{eff}}^{\uparrow\downarrow}$ for our Pt|Co samples and those of the other works cited here, indicate either a negative or at best a very large positive bare spin-mixing conductance $G^{\uparrow\downarrow}$.

Our conclusion is that the large values for $g_{\text{eff}}^{\uparrow\downarrow}$ (and hence either very high or negative apparent values for $G^{\uparrow\downarrow}$) extracted from the thickness dependent damping measurements for the Pt/Co series (E) and (F), and for the annealed CoFe/Pt series (D), are the result of some mechanism other than spin pumping into Pt through an abrupt, reasonably well ordered Pt/FM interface. One possibility we have considered is whether there is a significant SML at the interface of these Pt/FM bilayers that greatly enhances the effective spin conductance G'_{ext}. The presence of a SML layer, or at least interfacial disorder, in the annealed CoFe case seems consistent with the fact that the average resistivity of both the CoFe and Pt layers, as determined from conductance measurements of the bilayer films made as a function of t_{CoFe}, increases upon annealing [34]. The resistivity of the 4 nm Pt layer changes from $\rho_{\text{Pt}}^{\text{as-grown}} = 31.3\ \mu\Omega\text{cm}$ to $\rho_{\text{Pt}}^{\text{annealed}} = 32.8\ \mu\Omega\text{cm}$, while the resistivity of CoFe changes more substantially from $\rho_{\text{CoFe}}^{\text{as-grown}} = 40.7\ \mu\Omega\text{cm}$ to $\rho_{\text{CoFe}}^{\text{annealed}} = 48.2\ \mu\Omega\text{cm}$ which suggests increased disorder in the CoFe or some diffusion of Pt into the CoFe near the interface. However if we assume that $\theta_{\text{SH}}^{\text{Pt}} \approx 0.3$, as indicated by the ST-FMR results from the as-deposited CoFe samples, and use the result from the annealed CoFe samples that $\xi_{DL}^{\text{annealed}} = 0.077$, then we find that the trilayer model that yields Eqns. (3)-(5) can only provide a self-consistent solution if the spin mixing conductance for the CoFe/I interface is at least approximately ten times the Sharvin conductance of Pt [34], which again is unphysical. We conclude that the enhanced damping in this case cannot be due solely to spin pumping into and through a disordered interfacial layer between the CoFe and the Pt. A second alternative to consider is whether there is also strong spin scattering at the CoFe/SiO_2

interface of the annealed series (D) samples, perhaps associated in part with the enhancement of the dead layer thickness (from 0.3 nm to 0.7 nm) that is observed in those samples. In this case there still must be some enhanced spin scattering, SML, at the CoFe/Pt interface to account for the spin current attenuation there leading to the reduced spin torque efficiency $\xi_{DL}^{\text{annealed}} = 0.077$ in comparison to the as-deposited result, $\xi_{DL}^{\text{as-deposited}} = 0.10$. If we assume Eqn. (5) is applicable to this situation and that $G_{\text{I}} \approx G_{\text{Pt}}$ then a SML parameter $\delta \sim 1.9$ can account for the reduced spin torque efficiency for the annealed CoFe/Pt series (D) case.

Turning to the series (F) MgO/Co/Pt samples that have an ST-FMR response that indicates a constant $\xi_{DL} \approx 0.1$ over a Co thickness of 4 to 9 nm, we consider whether the high value of $g_{\text{eff}}^{\uparrow\downarrow} \approx 5.3\times10^{19}\,\text{m}^{-2}$ obtained from the damping measurements could be due to SML at the Co/Pt interface or to the t_d = 0.5 ± 0.2 dead layer that may be located in whole or in part at the MgO/Co interface. If we employ the SML parameters obtained from a recent low temperature giant magnetoresistance study of Pt/Co multilayers, $\delta = 0.9$ and $G_{\text{I}} \approx 1.2\times10^{15}\,\Omega^{-1}\text{m}^{-2}$ [36], with our measured value $g_{\text{eff}}^{\uparrow\downarrow} \approx 5.3\times10^{19}\,\text{m}^{-2}$, we obtain from Eqn. (5b) $\theta_{\text{SH}} \approx 1.1\,\xi_{DL}$ to $1.6\,\xi_{DL}$, depending on the assumed conductivity of the Pt ($\sigma_{\text{Pt}} \approx 3.2\times10^{6}\,\Omega^{-1}\text{m}^{-1}$ to $5.5\times10^{6}\,\Omega^{-1}\text{m}^{-1}$). However this value for G_{I} together with the measured $g_{\text{eff}}^{\uparrow\downarrow}$ once again requires (Eqn. (5)) the unphysical result that the spin-mixing conductance for this system be negative. If alternatively we conclude that the damping measurement here is not an accurate determination of $g_{\text{eff}}^{\uparrow\downarrow}$ and assume instead that the spin mixing conductance of the Co/Pt interface is approximately the same as we determined for the as-deposited CoFe/Pt interface, $G_{\text{CoFe,as-deposited}}^{\uparrow\downarrow} \approx 0.57\times10^{15}\,\Omega^{-1}\text{m}^{-2}$, then with these SML parameters and the measured $\xi_{DL} \approx 0.1$ Eqn. (5) predicts that $\theta_{\text{SH}}^{\text{Pt}} \approx 0.73$, a very high value which is not consistent with

the as-deposited CoFe/Pt or previously reported Py/Pt results. We conclude **(a)** that any SML at our Co/Pt interfaces is considerably less than that specified by the value $\delta = 0.9$ found in the previous low temperature magnetoresistance study [36], and in addition, **(b)** that the determination of $g_{\text{eff}}^{\uparrow\downarrow}$ from the FMR damping measurements is not always reliable. Our tentative explanation for the latter finding is that there must often be additional magnetic damping associated with one of or both of the FM interfaces in the Pt/FM samples, over and above the mechanism of spin pumping into the Pt. This extra magnetic damping might be generated at the surface of the FM opposite to the Pt layer or might be due to intermixing of Pt impurities within the magnetic layer near the FM/Pt interface. We do observe a correlation between the existence of enhanced damping and the presence of a magnetic dead layer in these samples (see Table 1); in particular the interfacial damping is greatly reduced in the as-deposited series (C) samples in which the apparent dead layer is smallest. The dead layer in the series (E) and (F) samples perhaps arises from some limited oxidation of the Co [41] facing the MgO, or some intermixing with the oxide during sputtering.

Summary and Conclusions

We have shown that there can be substantial variation in the efficiencies ξ_{DL} and ξ_{FL} of a current flowing in a Pt layer for exerting spin-orbit-induced torques on an adjacent FM layer via the spin Hall effect. For PM Pt/Co/MgO and Pt/CoFe/MgO (annealed) samples there is strong dependence on the FM thickness, with the results differing between the as-deposited Co samples and the annealed CoFe samples (in the latter case annealing was necessary to obtain PM). For our PM Pt/Co/MgO series (A) samples the highest $\xi_{DL} \approx 0.12$ is obtained in the thicker, ~ 1 nm, limit. For our annealed Pt/CoFe/MgO series (B) samples ξ_{DL} (and ξ_{FL}) drops substantially with increasing

thickness, possibly due to increasing spin memory loss at an increasingly disordered Pt/CoFe interface.

For the in-plane-magnetized samples the efficiencies of the spin-orbit torques vary substantially as a function of heat treatment (CoFe/Pt samples), and as a function of base layer and deposition order (Pt/Co samples). For the as-deposited CoFe/Pt series (C) samples we have "well-behaved" ST-FMR results indicating $\xi_{DL}^{\text{as-deposited}} \approx 0.10$ and only a quite small $\xi_{FL}^{\text{as-deposited}} \approx -0.004$. Annealing the CoFe/Pt samples reduces ξ_{DL} and increases ξ_{FL}. For the Pt/Co series of IPM samples the ST-FMR behavior differs when the Co layer is deposited on Pt (series (E)) and MgO (series F). The latter MgO/Co/Pt series (F) samples exhibit $\xi_{DL} \geq 0.10$, with the highest values being in the samples with the thinner Co and a very small ξ_{FL}. In contrast, the Pt/Co/MgO series (E) samples exhibit a reduced $\xi_{DL} \approx 0.065$ and a stronger field-like torque component, together with magnetic anisotropy behavior indicative of a strong interfacial magnetic energy density.

The spin torque measurements reported here set a lower bound on $\theta_{\text{SH}}^{\text{Pt}}$, the internal spin Hall angle of Pt with highest values $\xi_{DL} \approx 0.10 - 0.12$ being obtained from the PM Pt/Co/MgO series (A) samples and the as-deposited CoFe/Pt series (C) samples. However to relate these measured spin torque efficiencies to the actual internal spin Hall ratio of the Pt requires a quantification of the spin transparency of the interface. To obtain that we utilized in-plane-magnetized samples and attempted to determine the spin mixing conductance of the interface from spin pumping measurements. For the as-deposited CoFe/Pt samples we measured a low effective spin-mixing conductance, $g_{\text{eff, as-deposited}}^{\uparrow\downarrow} = 9.8 \times 10^{18}\,\text{m}^{-2}$, which is in reasonable accord with that calculated from first principles for Pt interfaces. If we assume no SML loss in the as-deposited CoFe/Pt case and a spin conductance for the Pt as calculated assuming the average conductivity of our Pt layer and $\lambda_{\text{s,Pt}} \approx 1.4\,\text{nm}$, we

obtain $\theta_{SH}^{Pt} \approx 0.33$. Of course any SML would only increase the amplitude of the true internal spin Hall angle.

When we use spin pumping measurements to determine the effective spin mixing conductance of the annealed CoFe/Pt samples, series (D), and the two types of Co/Pt samples, series (E) and series (F) the values we obtain, $g_{eff}^{\uparrow\downarrow} > 3\times10^{19}\,m^{-2}$, appear to be unphysical in that they require that either the spin mixing conductance of the interface be much more than the calculated Sharvin conductance of Pt, or, alternatively that there is a strong spin memory loss at the interface. However this latter alternative, in combination with the measured value of the spin torque efficiency, e.g. $\xi_{DL} \approx 0.1$ for the series (F) Co/Pt samples, requires that the spin Hall ratio of Pt >> 0.3. This is not consistent with the as-deposited CoFe/Pt result. This suggests an alternative source of surface (interface) enhanced damping, leading to an overestimate of the true $g_{eff}^{\uparrow\downarrow}$. Possible sources of this extra interfacial damping are mixing of Pt into the FM, and also some of the magnetic dead layer being on the opposite, oxide, surface of the FM. In support of this latter possibility we note that the samples with the high apparent $g_{eff}^{\uparrow\downarrow}$ also exhibit a relatively thick magnetic dead layer.

Finally we note that our conclusion that $\theta_{SH}^{Pt} \approx 0.3$ is quite different from a recent determination of the internal spin Hall angle of Pt based on an inverse spin Hall effect experiment, $\theta_{SH}^{Pt} = 0.056$ [17]. We do not have a good explanation for this strong disagreement but we do see that in [17] the reported effective spin-mixing conductance for the Co/Pt interface is $g_{eff,\,as\text{-}deposited}^{\uparrow\downarrow} = 8\times10^{19}\,m^{-2}$, much higher than the value we obtain for the as-deposited CoFe/Pt samples that have the cleanest ST-FMR results, and an overestimation of the spin mixing conductance would lead to an underestimation of θ_{SH}^{Pt} in an inverse spin Hall effect experiment.

Whatever the final resolution of the origin of these different experimental results, the demonstration here that the spin torque efficiency of both PM and IPM Pt/FM bilayers can, in some instances, be $\xi_{DL} \approx 0.10-0.12$ is quite promising for applications utilizing the SHE to generate spin torque. This work further demonstrates that the structure and quality of the NM/FM interface can play a critical role in determining the spin torque efficiency. Finally, our results, taken in total with other recent results [20-25], indicate that, depending on the exact spin conductance of the Pt film, the "internal" spin Hall angle of Pt could be as high as $\theta_{\mathrm{SH}}^{\mathrm{Pt}} \approx 0.30$ or even greater. This suggests that more effective and more energy-efficient spintronic devices might be realized by careful Pt/FM interfacial engineering, perhaps surpassing the overall performance of much-more-resistive spin Hall metals having large values of θ_{SH} (for instance β-Ta [8, 63] and β-W [9, 10, 64, 65]). Of course this then raises the interesting question as to whether the internal spin Hall angle of those latter two materials may also be higher than their measured spin torque efficiencies, or $\theta_{\mathrm{SH}}^{\mathrm{LB}}$. Further research may indeed prove this to be the case. However, we note that since the spin conductances of β-Ta and β-W both appear to be much lower than that of Pt, as indicated by their low $g_{\mathrm{eff}}^{\uparrow\downarrow}$ that is estimated from ST-FMR experiments with these metals, the spin transparency of either a β-Ta/FM [8] and β-W/FM [66] interface is likely to be closer to unity than that of a Pt/FM interface, and hence the measured $\theta_{\mathrm{SH}}^{\mathrm{LB}}$ closer to the true internal value.

C.-F. P. and Y. O. contributed equally to this work.

We would like to thank Graham Rowlands and Junbo Park for the assistance on low temperature measurements, Minh-Hai Nguyen for discussion on the spin-mixing conductance, and Praveen Gowtham for helpful discussion regarding magnetoelastic effects. We thank Stuart Parkin for sharing a manuscript reporting a related study prior to publication [26]. C.-F.P. thanks Satoru Emori for

fruitful discussion on proximity effect. This research was supported in part by NSF/MRSEC (DMR-1120296) through the Cornell Center for Materials Research (CCMR), by ONR, and by NSF through use of the Cornell Nanofabrication Facility (CNF)/NINN and the CCMR facilities.

*rab8@cornell.edu

References

[1] M. I. Dyakonov and V. I. Perel, Phys. Lett. A **35**, 459 (1971).
[2] J. E. Hirsch, Phys. Rev. Lett. **83**, 1834 (1999).
[3] L. Q. Liu, D. C. Ralph, and R. A. Buhrman, arXiv:1111.3702 (2011).
[4] J. Kim, J. Sinha, M. Hayashi, M. Yamanouchi, S. Fukami, T. Suzuki, S. Mitani, and H. Ohno, Nat. Mater. **12**, 240 (2013).
[5] K. Garello *et al.*, Nat. Nanotech. **8**, 587 (2013).
[6] K. Ando, S. Takahashi, K. Harii, K. Sasage, J. Ieda, S. Maekawa, and E. Saitoh, Phys. Rev. Lett. **101**, 036601 (2008).
[7] L. Q. Liu, T. Moriyama, D. C. Ralph, and R. A. Buhrman, Phys. Rev. Lett. **106**, 036601 (2011).
[8] L. Q. Liu, C.-F. Pai, Y. Li, H. W. Tseng, D. C. Ralph, and R. A. Buhrman, Science **336**, 555 (2012).
[9] C.-F. Pai, L. Q. Liu, Y. Li, H. W. Tseng, D. C. Ralph, and R. A. Buhrman, Appl. Phys. Lett. **101**, 122404 (2012).
[10] C.-F. Pai, M. H. Nguyen, C. Belvin, L. H. Vilela-Leao, D. C. Ralph, and R. A. Buhrman, Appl. Phys. Lett. **104**, 082407 (2014).
[11] I. M. Miron, G. Gaudin, S. Auffret, B. Rodmacq, A. Schuhl, S. Pizzini, J. Vogel, and P. Gambardella, Nat. Mater. **9**, 230 (2010).
[12] I. M. Miron *et al.*, Nat. Mater. **10**, 419 (2011).
[13] P. M. Haney, H. W. Lee, K. J. Lee, A. Manchon, and M. D. Stiles, Phys. Rev. B **87**, 174411 (2013).
[14] R. H. Liu, W. L. Lim, and S. Urazhdin, Phys. Rev. B **89**, 220409 (2014).
[15] X. Fan, J. Wu, Y. P. Chen, M. J. Jerry, H. W. Zhang, and J. Q. Xiao, Nat. Commun. **4**, 1799 (2013).
[16] T. X. Nan, S. Emori, C. T. Boone, X. J. Wang, T. M. Oxholm, J. G. Jones, B. M. Howe, G. J. Brown, and N. X. Sun, Phys. Rev. B **91**, 214416 (2015).
[17] J. C. Rojas-Sanchez *et al.*, Phys. Rev. Lett. **112**, 106602 (2014).
[18] Y. Liu, Z. Yuan, R. J. H. Wesselink, A. A. Starikov, and P. J. Kelly, Phys. Rev. Lett. **113**, 207202 (2014).
[19] Y. Y. Sun *et al.*, Phys. Rev. Lett. **111**, 106601 (2013).
[20] M. Althammer *et al.*, Phys. Rev. B **87**, 224401 (2013).
[21] S. Meyer, M. Althammer, S. Geprags, M. Opel, R. Gross, and S. T. B. Goennenwein, Appl. Phys. Lett. **104**, 242411 (2014).
[22] H. L. Wang, C. H. Du, Y. Pu, R. Adur, P. C. Hammel, and F. Y. Yang, Phys. Rev. Lett. **112**, 197201 (2014).
[23] M. Obstbaum, M. Hartinger, H. G. Bauer, T. Meier, F. Swientek, C. H. Back, and G. Woltersdorf, Phys. Rev. B **89**, 060407 (2014).
[24] L. Q. Liu, C. T. Chen, and J. Z. Sun, Nat. Phys. **10**, 561 (2014).
[25] M. Weiler, J. M. Shaw, H. T. Nembach, and T. J. Silva, Phys. Rev. Lett. **113**, 157204 (2014).
[26] W. Zhang, W. Han, X. Jiang, S.-H. Yang, and S. S. P. Parkin, Nat. Phys. **11**, 496 (2015).
[27] M. H. Nguyen, C.-F. Pai, D. C. Ralph, and R. A. Buhrman, Appl. Phys. Lett. **106**, 222402 (2015).
[28] Y. T. Chen, S. Takahashi, H. Nakayama, M. Althammer, S. T. B. Goennenwein, E. Saitoh, and G. E. W. Bauer, Phys. Rev. B **87**, 144411 (2013).

[29] A. Brataas, Y. V. Nazarov, and G. E. W. Bauer, Phys. Rev. Lett. **84**, 2481 (2000).
[30] K. Xia, P. J. Kelly, G. E. W. Bauer, A. Brataas, and I. Turek, Phys. Rev. B **65**, 220401 (2002).
[31] O. Mosendz, V. Vlaminck, J. E. Pearson, F. Y. Fradin, G. E. W. Bauer, S. D. Bader, and A. Hoffmann, Phys. Rev. B **82**, 214403 (2010).
[32] A. Azevedo, L. H. Vilela-Leao, R. L. Rodriguez-Suarez, A. F. L. Santos, and S. M. Rezende, Phys. Rev. B **83**, 144402 (2011).
[33] V. Vlaminck, J. E. Pearson, S. D. Bader, and A. Hoffmann, Phys. Rev. B **88**, 064414 (2013).
[34] See Supplementary Material for more details.
[35] C. T. Boone, H. T. Nembach, J. M. Shaw, and T. J. Silva, J. Appl. Phys. **113**, 153906 (2013).
[36] H. Y. T. Nguyen, W. P. Pratt Jr, and J. Bass, J. Magn. Magn. Mater. **361**, 30 (2014).
[37] U. H. Pi, K. W. Kim, J. Y. Bae, S. C. Lee, Y. J. Cho, K. S. Kim, and S. Seo, Appl. Phys. Lett. **97**, 162507 (2010).
[38] V. E. Demidov, S. Urazhdin, H. Ulrichs, V. Tiberkevich, A. Slavin, D. Baither, G. Schmitz, and S. O. Demokritov, Nat. Mater. **11**, 1028 (2012).
[39] R. H. Liu, W. L. Lim, and S. Urazhdin, Phys. Rev. Lett. **110**, 147601 (2013).
[40] S. Bandiera, R. C. Sousa, B. Rodmacq, and B. Dieny, IEEE Magnetics Letters **2**, 2174032 (2011).
[41] J. C. Read, P. G. Mather, and R. A. Buhrman, Appl. Phys. Lett. **90**, 132503 (2007).
[42] M. T. Johnson, P. J. H. Bloemen, F. J. A. denBroeder, and J. J. deVries, Rep. Prog. Phys. **59**, 1409 (1996).
[43] P. Chowdhury, P. D. Kulkarni, M. Krishnan, H. C. Barshilia, A. Sagdeo, S. K. Rai, G. S. Lodha, and D. V. S. Rao, J. Appl. Phys. **112**, 023912 (2012).
[44] A. V. Khvalkovskiy, V. Cros, D. Apalkov, V. Nikitin, M. Krounbi, K. A. Zvezdin, A. Anane, J. Grollier, and A. Fert, Phys. Rev. B **87**, 020402 (2013).
[45] O. Mosendz, J. E. Pearson, F. Y. Fradin, G. E. W. Bauer, S. D. Bader, and A. Hoffmann, Phys. Rev. Lett. **104**, 046601 (2010).
[46] K. Ando *et al.*, J. Appl. Phys. **109**, 103913 (2011).
[47] S. Emori, U. Bauer, S. M. Ahn, E. Martinez, and G. S. D. Beach, Nat. Mater. **12**, 611 (2013).
[48] O. J. Lee, L. Q. Liu, C. F. Pai, Y. Li, H. W. Tseng, P. G. Gowtham, J. P. Park, D. C. Ralph, and R. A. Buhrman, Phys. Rev. B **89**, 024418 (2014).
[49] M. D. Stiles and A. Zangwill, Phys. Rev. B **66**, 014407 (2002).
[50] J. Kim, J. Sinha, S. Mitani, M. Hayashi, S. Takahashi, S. Maekawa, M. Yamanouchi, and H. Ohno, Phys. Rev. B **89**, 174424 (2014).
[51] X. P. Qiu, P. Deorani, K. Narayanapillai, K. S. Lee, K. J. Lee, H. W. Lee, and H. Yang, Scientific Reports **4**, 4491 (2014).
[52] V. M. Edelstein, Solid State Comm. **73**, 233 (1990).
[53] S. Bandiera, R. C. Sousa, B. Rodmacq, and B. Dieny, Appl. Phys. Lett. **100**, 142410 (2012).
[54] T. D. Skinner, M. Wang, A. T. Hindmarch, A. W. Rushforth, A. C. Irvine, D. Heiss, H. Kurebayashi, and A. J. Ferguson, Appl. Phys. Lett. **104**, 062401 (2014).
[55] A. R. Mellnik *et al.*, Nature **511**, 449 (2014).
[56] Y. Tserkovnyak, A. Brataas, and G. E. W. Bauer, Phys. Rev. Lett. **88**, 117601 (2002).
[57] Y. Tserkovnyak, A. Brataas, and G. E. W. Bauer, Phys. Rev. B **66**, 224403 (2002).
[58] F. D. Czeschka *et al.*, Phys. Rev. Lett. **107**, 046601 (2011).
[59] M. Weiler *et al.*, Phys. Rev. Lett. **111**, 176601 (2013).
[60] M. Zwierzycki, Y. Tserkovnyak, P. J. Kelly, A. Brataas, and G. E. W. Bauer, Phys. Rev. B **71**, 064420 (2005).

[61] Y. Tserkovnyak, A. Brataas, G. E. W. Bauer, and B. I. Halperin, Rev Mod Phys **77**, 1375 (2005).
[62] S. Mizukami, E. P. Sajitha, D. Watanabe, F. Wu, T. Miyazaki, H. Naganuma, M. Oogane, and Y. Ando, Appl. Phys. Lett. **96**, 152502 (2010).
[63] M. Cubukcu *et al.*, Appl. Phys. Lett. **104**, 042406 (2014).
[64] Q. Hao and G. Xiao, Phys. Rev. Applied **3**, 034009 (2015).
[65] Q. Hao, W. Chen, and G. Xiao, Appl. Phys. Lett. **106**, 182403 (2015).
[66] Y. Li, PhD Dissertation, Cornell University, 2014

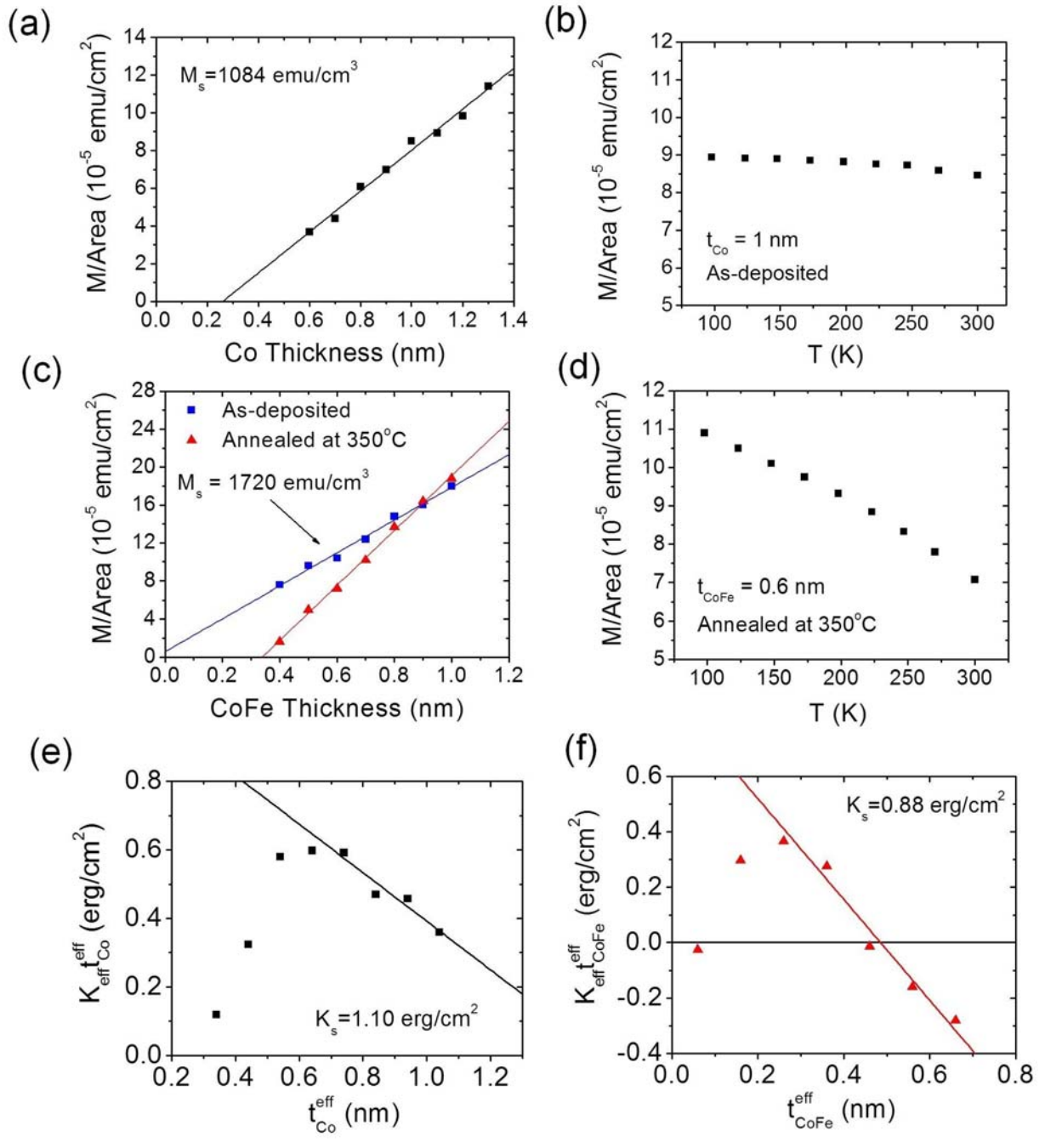

FIG. 1 (color online). (a) The magnetic moment per unit area as a function of sputtered Co thickness in Pt/Co/MgO samples. (b) Temperature dependence of the magnetic moment per unit area in Pt/Co/MgO sample with 1 nm of Co. (c) The magnetic moment per unit area as a function of sputtered CoFe thickness in both as-deposited (blue squares) and annealed (red triangles) Pt/Co/MgO

samples. (d) Temperature dependence of the magnetic moment per unit area in annealed Pt/CoFe/MgO sample with 0.6 nm of CoFe. The effective magnetic anisotropy energy density in terms of $K_{\text{eff}} t_{FM}^{\text{eff}}$ (e) for as-deposited Pt/Co/MgO as a function of effective Co thickness and (f) for annealed Pt/CoFe/MgO as a function of effective CoFe thickness. K_s indicates the interfacial anisotropy energy obtained from the intercept of the linear fit (solid lines).

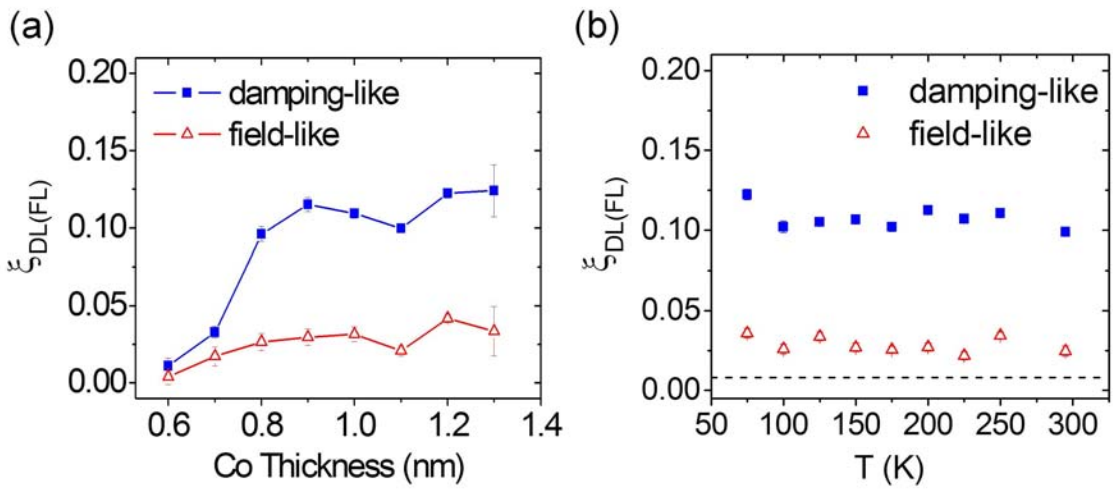

FIG. 2 (color online). (a) The damping-like (field-like) torque efficiency $\xi_{DL(FL)}$ of Pt from as-deposited Pt/Co/MgO series (A) samples as a function of Co thickness. Representative error bars due to the device-to-device variation are shown on the data from samples with 1.3 nm of Co. Smaller error bars for other data represent the uncertainties due to fitting. (b) $\xi_{DL(FL)}$ of Pt from a representative Pt(4)/Co(1)/MgO(2) series (A) sample as a function of temperature T. The blue squares and the red triangles represent data for the damping-like torque and from field-like torque, respectively. For comparison, a dashed line is shown in (b) to indicate the sign and the magnitude of the Oersted field expressed in terms of a spin torque efficiency.

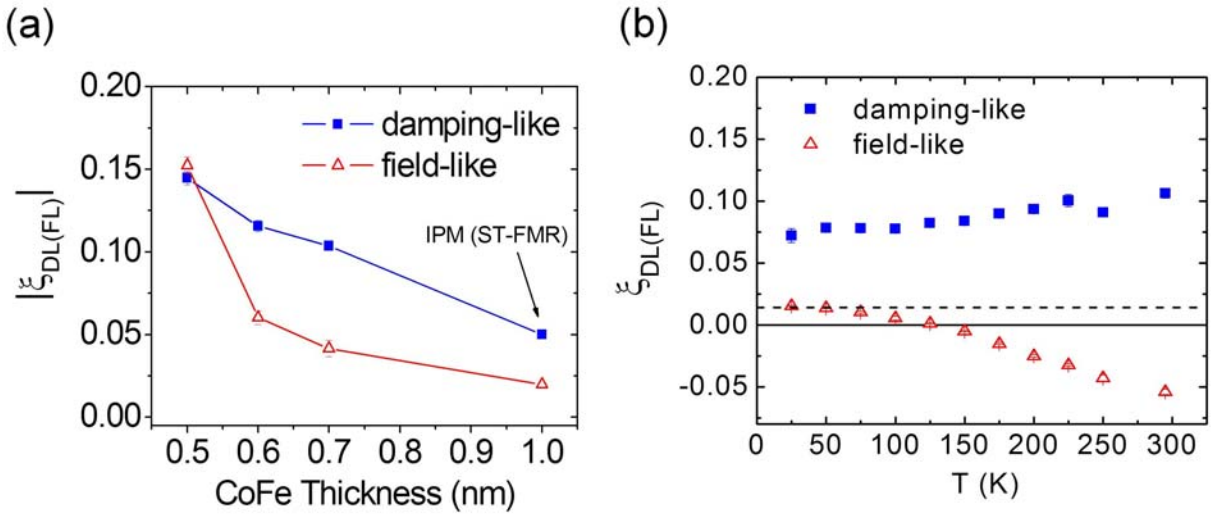

FIG. 3 (color online). (a) The damping-like (field-like) torque efficiency $\xi_{DL(FL)}$ of Pt from Pt/CoFe/MgO series (B) samples annealed at 350°C as a function of CoFe thickness. The blue squares and the red triangles represent data for the damping-like torque and the field-like torque, respectively. The data for 1 nm of CoFe were obtained from ST-FMR measurements on IPM samples, while the rest were obtained from HR measurements on PM samples. (b) $\xi_{DL(FL)}$ of Pt from a representative Pt(4)/CoFe(0.6)/MgO(2) series (B) sample as a function of temperature T. For comparison, a dashed line is shown to indicate the sign and the magnitude of the Oersted field in terms of a spin torque efficiency.

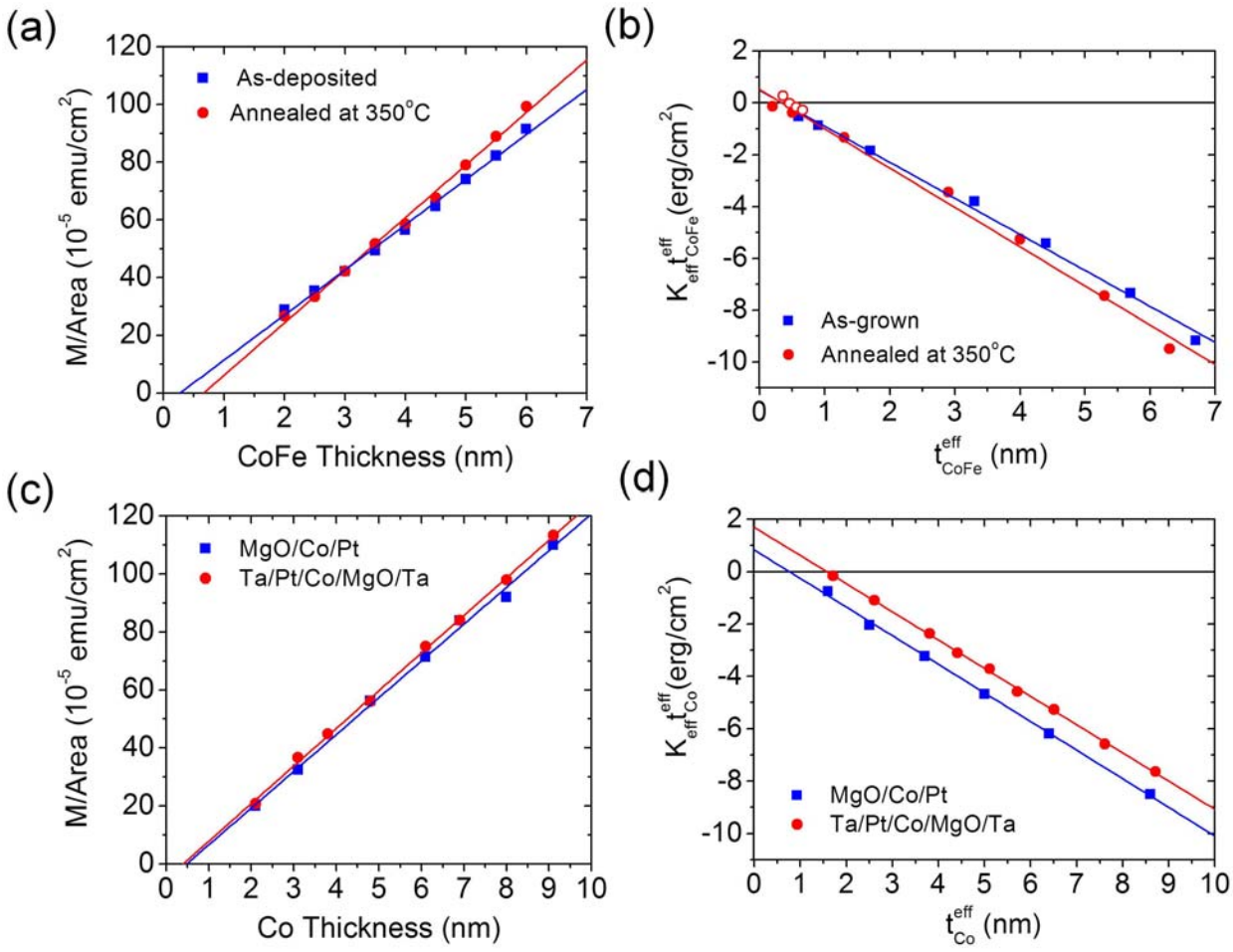

FIG. 4 (color online). (a) The magnetic moment per unit area as a function of CoFe thickness in IPM as-deposited CoFe/Pt series (C) (blue squares) and annealed CoFe/Pt series (D) (red circles) samples. (b) The effective magnetic anisotropy energy density of as-deposited CoFe/Pt series (C) (blue squares) and annealed CoFe/Pt series (D) (red circles) samples plotted in terms of $K_{\text{eff}}t_{\text{CoFe}}^{\text{eff}}$ as a function of effective CoFe thickness $t_{\text{CoFe}}^{\text{eff}}$. The red open circles represent data from annealed PM Pt/CoFe/MgO series (B) samples. (c) The magnetic moment per unit area as a function of Co thickness in Ta/Pt/Co/MgO/Ta series (E) (red circles) and MgO/Co/Pt series (F) (blue squares) samples. (d) The effective magnetic anisotropy energy density of Ta/Pt/Co/MgO/Ta series (E) (red circles) and MgO/Co/Pt series (F) (blue squares) samples plotted in terms of $K_{\text{eff}}t_{\text{Co}}$ as a function of

effective Co thickness $t_{\mathrm{Co}}^{\mathrm{eff}}$.

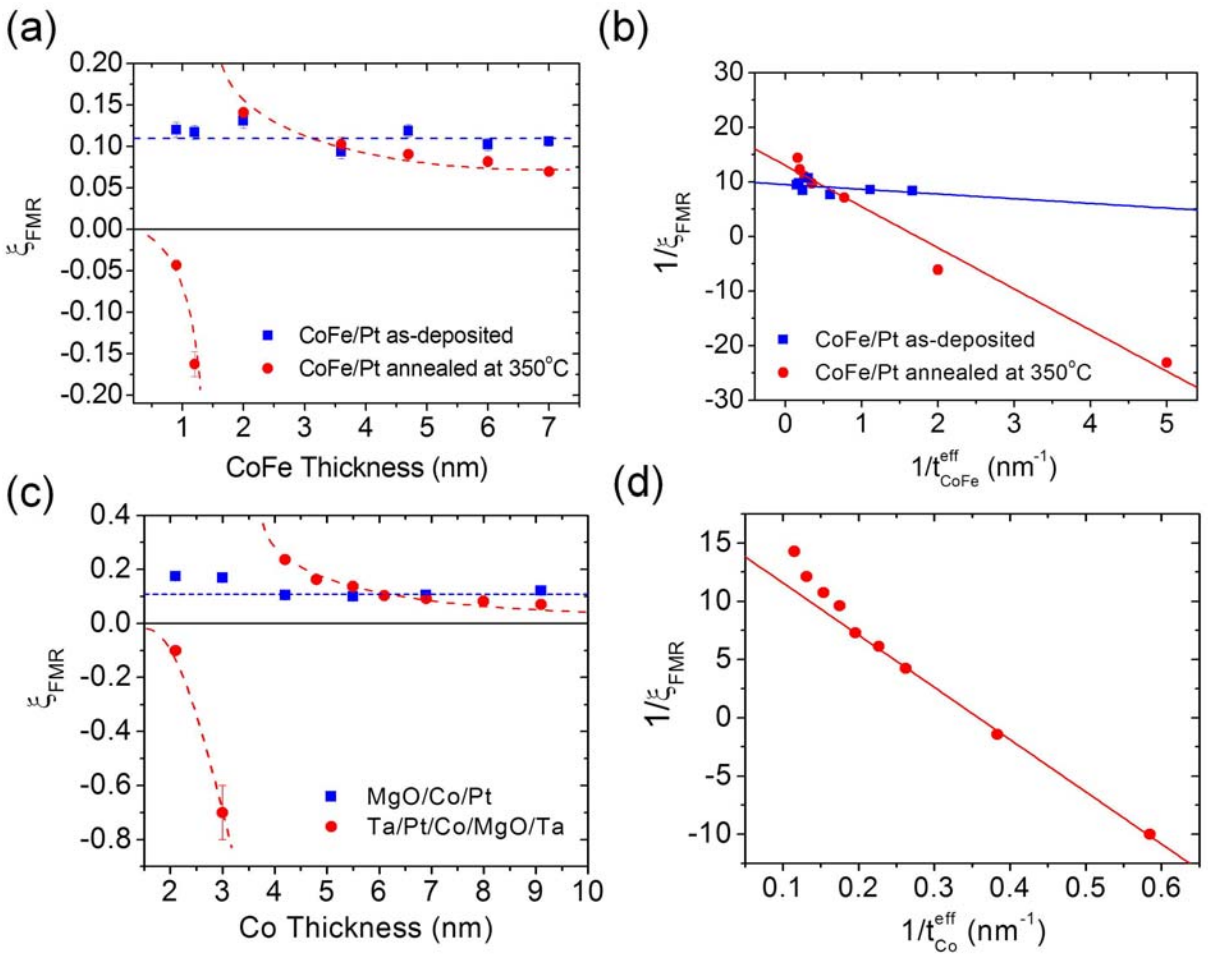

FIG. 5 (color online). (a) The ST-FMR apparent spin torque efficiency ξ_{FMR} of Pt from IPM CoFe/Pt series (C) and (D) samples as a function of CoFe thickness . The blue and red dashed lines serve as guides to eye for the as-deposited and annealed CoFe/Pt data, respectively. (b) The inverse of the ST-FMR apparent spin torque efficiency, $1/\xi_{FMR}$, as a function of the inverse of the effective CoFe layer thickness $1/t_{\mathrm{CoFe}}^{\mathrm{eff}}$ for the series (C) and (D) samples, with linear fits. (c) ξ_{FMR} of Pt from IPM Ta/Pt/Co/MgO series (E) samples and MgO/Co/Pt series (F) samples as a function of Co thickness. The blue and red dashed lines serve as guides to eye for the MgO/Co/Pt and Ta/Pt/Co/MgO data,

respectively. (d) The inverse of the ST-FMR apparent spin torque efficiency, $1/\xi_{FMR}$, for the Ta/Pt/Co/MgO series (E) samples as a function of $1/t_{\mathrm{Co}}^{\mathrm{eff}}$. The solid line represents a linear fit.

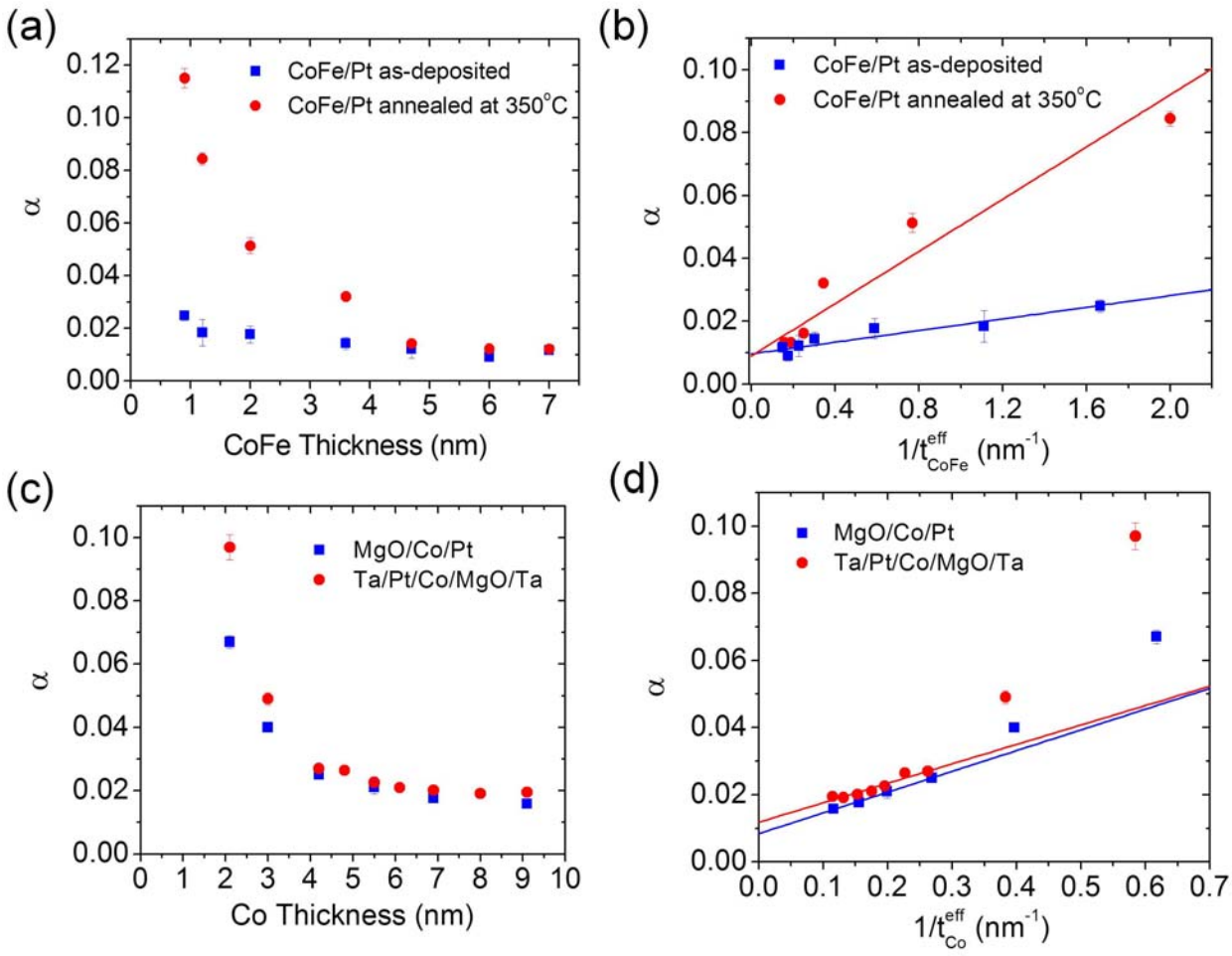

FIG. 6 (color online). (a,b) The damping constant α of CoFe from the as-deposited CoFe/Pt series (C) samples (blue squares) and annealed CoFe/Pt series (D) samples (red circles) as a function of (a) CoFe thickness and (b) the inverse of the effective CoFe thickness $1/t_{\mathrm{CoFe}}^{\mathrm{eff}}$. The solid lines represent linear fits. (c,d) The damping constant α of Co from the Ta/Pt/Co/MgO series (E) samples (red circles) and from the MgO/Co/Pt series (F) samples (blue squares) as a function of (c) Co thickness and (d) the inverse of the effective Co thickness $1/t_{\mathrm{Co}}^{\mathrm{eff}}$. The solid lines represent linear fits to the data in the thick Co regime ($t_{\mathrm{Co}}^{\mathrm{eff}} \geq 3$ nm).

Series	Layer Structure	t_{FM} (nm)	Heat Treatment	t_D (nm)	M_s (emu/cm^3)	K_S (ergs/cm^2)	ξ_{DL}	ξ_{FL}	$g_{eff}^{\uparrow\downarrow}$ (nm^{-2})
	Perpendicularly Magnetized								
(A)	||Ta(2)/Pt(4)/Co(t_{Co})/MgO(2)/Ta(1)	0.5-1.3	as-deposited	0.26	1084	1.10	0.12 (max)	0.03 (max)	n.a.
(B)	||Ta(2)/Pt(4)/$Co_{50}Fe_{50}$(t_{CoFe})/MgO(2)/Ta(1)	0.4-1.1	annealed (350°C)	0.34	2884	0.88	0.15 (max)	-0.15 (max)	n.a.
	In-Plane Magnetized								
(C)	||$Co_{50}Fe_{50}$(t_{CoFe})/Pt(4)	1-9	as-deposited	0.30	1560	0.48	0.10	-0.004	9.8
(D)	||$Co_{50}Fe_{50}$(t_{CoFe})/Pt(4)	1-9	annealed (350°C)	0.70	1820	0.52	0.077	-0.011	51
(E)	||Ta(2)/Pt(4)/Co(t_{Co})/MgO(2)/Ta(1)	2-9	as-deposited	0.39	1290	1.70	0.064	-0.029	51
(F)	||MgO(1.6)/Co(t_{Co})/Pt(4)	2-9	as-deposited	0.50	1270	0.84	0.10	< -0.01	53

Table I. A summary of the parameters of the different series of samples in this study: Here t_{FM} is the thickness of the ferromagnetic layer, t_D is the apparent magnetic dead layer thickness as determined by thickness dependent measurement of the film magnetic moments, M_s is the apparent saturation magnetization of the ferromagnetic layer, K_s is the interfacial anisotropy energy density of the FM as determined by SQUID magnetometry for the perpendicularly magnetized samples and by spin torque FMR measurement of the demagnetization field ($4\pi M_{eff}$) for the in-plane magnetized samples, ξ_{DL} and ξ_{FL} are, respectively, the damping-like and field-like spin torque efficiencies of each series, and $g_{eff}^{\uparrow\downarrow}(\mathrm{nm}^{-2})$ is the apparent effective spin mixing conductance as determined by thickness dependent measurement of the FMR linewidth (spin pumping effect).